SF2A 2021
A. Siebert, K. Baillié, E. Lagadec, N. Lagarde, J. Malzac, J.-B. Marquette, M. N'Diaye, J. Richard, O. Venot (eds)

REVIVAL OF INTENSITY INTERFEROMETRY WITH MODERN PHOTONIC TECHNOLOGIES

W. Guerin[1], J.-P. Rivet[2], M. Hugbart[1], F. Vakili[2,3], E. S. G. de Almeida[2], A. Domiciano de Souza[2], G. Labeyrie[1], N. Matthews[1], O. Lai[2], P.-M. Gori[2], D. Vernet[4], J. Chabé[5], C. Courde[5], E. Samain[6], B. V. Castilho[7], A. M. Magalhaes[8], E. Janot-Pacheco[8], A. Carciofi[8], P. Bourget[9], N. Schuhler[9] and R. Kaiser[1]

Abstract. We present our project on the revival of intensity interferometry with modern photonic technologies, and more specifically with conventional optical telescopes. This original approach is complementary to the work currently done aiming at applying intensity interferometry to Cherenkov telescopes. We briefly summarize the results obtained so far.

Keywords: Intensity interferometry, Correlation function, η Carinæ

1 Introduction

The study of light intensity correlations, while being nowadays the daily bread of quantum opticians, was originally pioneered by R. Hanbury Brown and R. Q. Twiss for astronomy (Hanbury Brown & Twiss 1956). Indeed, they demonstrated that the intensity correlation function $g^{(2)}(r,\tau)$ (Guerin et al. 2018) provides information about the source: the amplitude of the "bunching peak", i.e., $g(r,\tau=0)-g(r,\tau\to\infty)$, is proportional to the squared modulus of the visibility. This technique was called stellar intensity interferometry (SII), as opposed to amplitude (or direct or Michelson) interferometry, in which the visibility is measured by the contrast of the interference fringes. Direct optical interference is challenging as it requires a control of the optical paths to better precision than the wavelength. On the contrary, SII is relatively insensitive to the phase of the optical field and therefore much easier to implement. However, this simplicity has a price of lower sensitivity in comparison to direct inteferometry. Therefore, SII requires large collectors and has only so far been used with very bright stars (Hanbury Brown et al. 1974).

Nevertheless, for the last 15 years, there has been a growing interest in reviving SII, in particular in the context of the future Cherenkov Telescope Array (CTA) [see, e.g., (Dravins et al. 2013) and references therein]. Indeed, the number and size of baselines would be much greater than with any other interferometer, with an unprecedented collecting surface. Recently, successful measurements have been performed with other Cherenkov telescopes, namely the MAGIC array (Acciari et al. 2020) and the VERITAS array (Abeysekara et al. 2020).

Our team follows a complementary approach, which is to revive SII for optical telescopes (Rivet et al. 2018). Although the size and number of available telescopes will probably always be much smaller than with Cherenkov arrays, the optical quality of the telescopes provides several advantages. The seeing-limited point-spread function (PSF) (compared with a typical PSF of 0.1° of Cherenkov telescopes) allow us to use the

[1] Université Côte d'Azur, CNRS, Institut de Physique de Nice, France
[2] Université Côte d'Azur, Observatoire de la Côte d'Azur, CNRS, Laboratoire Lagrange, France
[3] Department of Physics, Shahid Beheshti University, G.C., Tehran, Iran
[4] Université Côte d'Azur, Observatoire de la Côte d'Azur, CNRS, UMS Galilée, France
[5] Université Côte d'Azur, Observatoire de la Côte d'Azur, CNRS, Laboratoire Géoazur, France
[6] SigmaWorks, Saint Vallier de Thiey, France
[7] Laboratório Nacional de Astrofísica, Brazil
[8] Instituto de Astronomia, Geofisica e Ciências Atmosféricas, Universidade de São Paulo, Brazil
[9] European Southern Observatory, Chile

best available detectors, yielding a better quantum efficiency ($>70\%$) and timing resolution ($<500\,$ps), and to transport the light from the telescope focus to the detectors by optical fibers. It also allows us to use narrow-band filters (e.g., $\Delta\lambda \leq 1\,$nm) to increase the coherence time, and select emission lines. In that configuration stray light from the sky background is negligible. In the future, this should also allow us to use integrated photonic components (Dinkelaker et al. 2021), for example for wavelength multiplexing (Lai et al. 2018). Finally, our setup is compact and transportable and can easily be adapted to any facility.

In this paper we briefly summarize the status of our project and the results obtained so far. Note that in parallel we are also contributing to the study on the use of Cherenkov telescope for SII (Gori et al. 2021).

2 Results

2.1 Experimental setup

Our setup is based on avalanche photodiodes (APDs) used in photon counting mode. Counting and correlations are performed in real time by a time-to-digital converter (TDC). In order to measure the zero-baseline $g^{(2)}(\tau, r = 0)$ correlation function, two APDs per channel are required, each one fed by the complementary outputs of a fibered 50:50 splitter. Special care is taken to avoid spurious correlations and crosstalk.

The inputs of the fibered splitters are connected to optical telescopes output ports through multimode graded index optical fibers (MMF) with $100\,\mu$m core diameter. Fig. 1 describes the optical interfaces we use to couple the fiber tips to the output beams of the telescopes. The converging beam issued by the telescope first passes through a dichroic beam splitter (DBS). The blue part of the light is reflected to a guiding CCD camera, through a neutral density filter (ND). The red part is transmitted to the collimating lens L_1. The collimated beam passes through a narrow-band filter ($\Delta\lambda = 1\,$nm) to increase the coherence time or select an emission line. Then, a polarizing beam splitter (PBS) separates the light into two orthogonal linear polarization states denoted as "V" and "H" for the reflected and transmitted beams, respectively. An additional linear polarizing plate is placed in the path of the reflected beam to increase the extinction ratio, which would otherwise be significantly lower than for the transmitted beam. A converging lens L_2 is then used to efficiently inject the filtered light into the MMFs. The combination of the collimation and focusing lenses results in a focal reduction factor of 2.5. These coupling modules are made almost completely from standard off-the-shelf opto-mechanical components, requiring only a few custom mechanical adaptation parts.

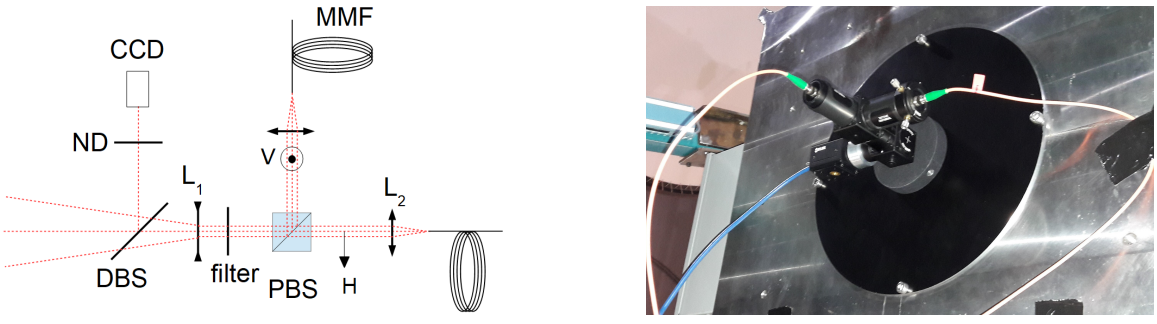

(a) (b)

Fig. 1: (a) Scheme of the coupling module at the focus of the telescope, as it was in 2018-2019. The previous version only had one polarization channel and converging light on the filter; in the next version we have added a supplementary linear polarizer on the V channel to improve the purity of the polarization. (b) Picture of the coupling module at the Nasmyth focus of the SOAR telescope.

2.2 Temporal and spatial bunching with star light

Our first on-sky test of intensity correlation measurements were performed in February 2017 using a 1 m telescope of the C2PU facility (Observatoire de la Côte d'Azur, Calern site). For this initial experiment, we measured the temporal correlation function $g^{(2)}(\tau)$, yielding a zero-baseline calibration ($r = 0$). We obtained well-resolved bunching peaks on three different very bright stars (Arcturus, Procyon and Pollux) at $\lambda = 780\,$nm. We could also estimate the injection efficiency into the MMF to be $\sim 66\%$ for average seeing conditions ($\sim 1.4''$) and

check that the signal-to-noise (SNR) ratio was only limited by the photon statistics (Guerin et al. 2017). This means that we can always look at dimer objects at the cost of a longer integration time.

In October 2017 we duplicated the coupling module and performed a spatial SII experiment between the two C2PU telescopes separated by 15 m. We observed bunching peaks with two marginally resolved bright stars, Vega and Rigel, and also with a more complex, partially resolved target, the Capella binary, yielding a reduced visibility (Guerin et al. 2018).

2.3 Intensity interferometry on emission lines

The narrow spectral filtering is particularly well adapted to select emission lines allowing for the study of extended stellar atmospheres. This naturally includes Hα emission, but also lines at shorter wavelengths such as Hβ, or He lines, which are traditionally challenging to observe with direct interferometry. The use of such narrow filters is difficult in Cherenkov telescopes due to the large PSF and has so far been limited to $\Delta\lambda > 10$ nm. Therefore interferometry on emission lines at short wavelengths is a natural niche for SII with optical telescopes.

In August 2018 we have performed a run of observations on the very intense Hα emission line of P Cygni. We obtained normalized squared visibilities on the order of 0.3 to 0.5 for baselines between 12 and 15 m. These visibilities are related to the angular size of the emissive region. We used the radiative transfer code CMFGEN (Hillier & Miller 1998) to model the star. We tuned some parameters to reproduce a spectrum acquired independently, which then allowed us to compute the luminosity profile (and thus the physical size) of the star. The Hankel transform of this model profile can thus be adjusted to the visibility data with the distance of the star as the only free parameter. This procedure allowed us to determine P Cygni's distance with an uncertainty comparable with the best published values (Rivet et al. 2020).

2.4 Observations at SOAR

In April 2019 we had one allocated night (at full moon) on the 4.1 m Southern Astrophysical Research (SOAR) Telescope in Chile. It was a single-telescope experiment, yielding the temporal correlation function, like in (Guerin et al. 2017). The goal was mainly to demonstrate the transportability and adaptability of our setup. In order to adapt the setup from the C2PU telescopes (diameter 1.06 m, focal length 13 m) to the SOAR telescope (diameter 4.1 m, focal length 68.175 m) we only had to add a converging lens ($f = 200$ mm) at the input of the coupling module in order to reduce the global focal length. This was also the first time we performed simultaneous measurements with two polarization channels. It is interesting to note that all our equipment was carried in two suitcases only, emphasizing the simplicity and compactness of the setup.

The target was the Hα line of η Carinæ with a total observing time of only 3.5 hours due to a partly cloudy night. The average count rate was about 4.5×10^6 counts per second per detector on each polarization channel, with a significant defocussing not to saturate the detectors. The results for the two polarization channels are presented in Fig. 2. One can see that the widths and the heights are different on the two functions, and they do not agree with each other within the uncertainties. This is mainly due to the fact that each APD has a different jitter such that each detector pair has a different timing resolution. However, the area of the bunching peak should remain constant against differences in the detector jitter and thus we use the area as our observable.

The area under each peak is extracted from a Gaussian fit. We get $A_{\mathrm{H}} = 0.68 \pm 0.13$ ps and $A_{\mathrm{V}} = 0.60 \pm 0.13$ ps, with 1σ statistical uncertainties. The two areas are in agreement within the error bars, although we found out later that there is a systematic underestimation of the bunching area on the V-channel, estimated

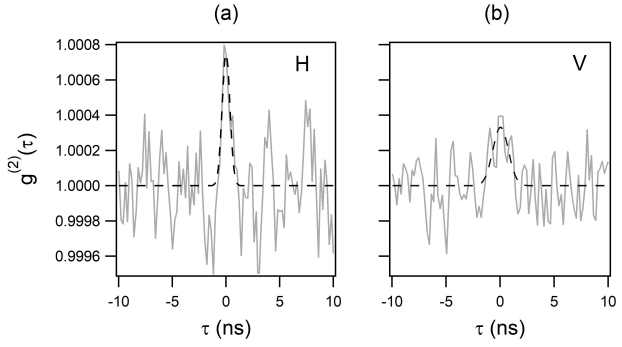

Fig. 2: Temporal intensity correlation functions measured on η Car in the night of 19/20 April 2019. (a) Horizontal polarization channel. (b) Vertical polarization channel. Dashed lines: Gaussian fits.

at $\sim 20\%$ by lab calibration. Half of this reduction can be attributed to the extinction ratio of the PBS, which can be as low as $1:20$ (while it's much better in transmission for the H channel). Indeed, 5% of orthogonal polarization induce a loss of coherence of 10%. The origin of the other missing 10% is not known with certainty but could be due to a slow tail in the timing response of one of the detectors. By correcting for this loss of contrast, and taking the weighted average of the two measurements, our final estimation of the bunching peak area is $A = 0.7 \pm 0.1$ ps.

To calculate the expected area of the bunching peak, we need to numerically compute the $g^{(2)}(\tau)$ function from a measured spectrum, as explained in (Rivet et al. 2020). Although the source is variable, we have checked that several spectra found in open data bases give very close results. We find an expected bunching area equal to $A_0 = 1.48$ ps, significantly higher than our measured value $A = 0.7 \pm 0.1$ ps. This indicates that the 4.1 m aperture of the telescope partially resolves the Hα-emitting region.

Since we know the telescope's aperture, we could compute the expected visibility, given a model for the shape of the emissive region. If there is only one free parameter in the model [like the distance in (Rivet et al. 2020), also using the spectrum to constrain the model], such measurement would allow us to fit this parameter. This is beyond the scope of this paper because η Car is a highly complex object and our measurement uncertainty is still relatively high, due to the short integration time and poor weather conditions.

3 Prospects

Recently, we have improved the optical quality of our coupling module and upgraded it with a tip-tilt correction, which will improve the average injection efficiency in the fibers. We have also performed some tests of superconducting nanowire single-photon detectors [SNSPDs, Zadeh et al. (2021)], which are very promising for SII. On the long term, the way to significantly increase the sensitivity is to perform multichannel measurements, and we start exploring the possible techniques to do it (Lai et al. 2018).

Another direction is to extend the number and size of available baselines. For that we plan to use a transportable 1 m telescope at Calern and the 1.5 m laser-ranging telescope, which is located 150 m away from the C2PU telescopes. We have already developed and tested a method to transfer the timing signal at this long distance with a few picosecond accuracy. We also plan to perform experiments using the Auxiliary Telescopes (ATs) of the VLTI (Chile), which have the strong advantage of being movable. The opto-mechanical adaption of our coupling module to the ATs has already been done. Initial on-sky tests with the ATs are provisionally scheduled for February 2022.

Finally, another (more speculative) goal is to search for laser-like emission (Johansson & Letokhov 2007).

We thank J. Elias, A. Tokovinin, and all the technical staff at SOAR for their help before and during our observing session. We acknowledge the financial support of the UCA-JEDI (ANR-15-IDEX-01), the Doeblin Federation (FR2800 CNRS), the OPTIMAL platform, the Région PACA (project I2C) and the French National Research Agency (project I2C No. ANR-20-CE31-0003).

References

Abeysekara, A. U., Benbow, W., Brill, A., et al. 2020, Nature Astronomy, 4, 1164

Acciari, V. A., Bernardos, M. I., Colombo, E., et al. 2020, MNRAS, 491, 1540

Dinkelaker, A. N., Rahman, A., Bland-Hawthorn, J., et al. 2021, Appl. Opt., 60, AP1

Dravins, D., LeBohec, S., Jensen, H., & Nuñez, P. D. 2013, Astropart. Phys., 43, 331

Gori, P.-M., Vakili, F., Rivet, J.-P., et al. 2021, MNRAS, 505, 2328

Guerin, W., Dussaux, A., Fouché, M., et al. 2017, MNRAS, 472, 4126

Guerin, W., Rivet, J.-P., Fouché, M., et al. 2018, MNRAS, 480, 245

Hanbury Brown, R., Davis, J., & Allen, L. R. 1974, MNRAS, 167, 121

Hanbury Brown, R. & Twiss, R. Q. 1956, Nature, 178, 1046

Hillier, D. J. & Miller, D. L. 1998, ApJ, 496, 407

Johansson, S. & Letokhov, V. S. 2007, New. Astron. Rev., 51, 443

Lai, O., Guerin, W., Vakili, F., et al. 2018, in Optical and Infrared Interferometry and Imaging VI, Vol. 10701, Proc. SPIE, 1070121

Rivet, J.-P., Siciak, A., de Almeida, E. S. G., et al. 2020, MNRAS, 494, 218

Rivet, J.-P., Vakili, F., Lai, O., et al. 2018, Exp. Astron., 46, 531

Zadeh, I. E., Chang, J., Los, J. W. N., et al. 2021, Appl. Phys. Lett., 118, 190502